Popeye domain containing proteins are essential for stress-mediated modulation of cardiac pacemaking in mice

Alexander Froese,[1] Stephanie S. Breher,[1] Christoph Waldeyer,[2] Roland F.R. Schindler,[1] Viacheslav O. Nikolaev,[3] Susanne Rinné,[4] Erhard Wischmeyer,[5] Jan Schlueter,[1] Jan Becher,[6] Subreena Simrick,[7] Franz Vauti,[8] Juliane Kuhtz,[1] Patrick Meister,[1] Sonja Kreissl,[1] Angela Torlopp,[1] Sonja K. Liebig,[2] Sandra Laakmann,[2] Thomas D. Müller,[9] Joachim Neumann,[10] Juliane Stieber,[11] Andreas Ludwig,[11] Sebastian K. Maier,[6] Niels Decher,[4] Hans-Henning Arnold,[8] Paulus Kirchhof,[2] Larissa Fabritz,[2] and Thomas Brand[1]

[1]Cell and Developmental Biology, University of Würzburg, Würzburg, Germany. [2]Department of Cardiology and Angiology, University Hospital Münster and IZKF Münster, Münster, Germany. [3]Institute of Pharmacology and Toxicology, University of Würzburg, Würzburg, Germany. [4]Institute for Physiology and Pathophysiology, Vegetative Physiology, University of Marburg, Marburg, Germany. [5]Institute of Physiology II, University of Würzburg, Würzburg, Germany. [6]Department of Internal Medicine I, University Hospital Würzburg, Würzburg, Germany. [7]Heart Science Centre, Imperial College London, Harefield, United Kingdom. [8]Cell and Molecular Biology, University of Braunschweig, Braunschweig, Germany. [9]Molecular Plant Physiology and Biophysics, University of Würzburg, Würzburg, Germany. [10]Institute of Pharmacology and Toxicology, University of Halle-Wittenberg, Halle, Germany. [11]Institute of Experimental and Clinical Pharmacology and Toxicology, University of Erlangen-Nürnberg, Erlangen, Germany.

Cardiac pacemaker cells create rhythmic pulses that control heart rate; pacemaker dysfunction is a prevalent disorder in the elderly, but little is known about the underlying molecular causes. Popeye domain containing (Popdc) genes encode membrane proteins with high expression levels in cardiac myocytes and specifically in the cardiac pacemaking and conduction system. Here, we report the phenotypic analysis of mice deficient in *Popdc1* or *Popdc2*. ECG analysis revealed severe sinus node dysfunction when freely roaming mutant animals were subjected to physical or mental stress. In both mutants, bradyarrhythmia developed in an age-dependent manner. Furthermore, we found that the conserved Popeye domain functioned as a high-affinity cAMP-binding site. Popdc proteins interacted with the potassium channel TREK-1, which led to increased cell surface expression and enhanced current density, both of which were negatively modulated by cAMP. These data indicate that Popdc proteins have an important regulatory function in heart rate dynamics that is mediated, at least in part, through cAMP binding. Mice with mutant *Popdc1* and *Popdc2* alleles are therefore useful models for the dissection of the mechanisms causing pacemaker dysfunction and could aid in the development of strategies for therapeutic intervention.

Introduction

Cardiac myocytes are able to conduct electrical activity. However, only specialized pacemaker myocytes, which are located in the sinus node, are normally able to initiate cardiac action potentials (1). Nodal myocytes are small, have few myofibrils, and are electrically poorly coupled (2). At the gene expression level, the sinus node and working myocardium display mostly quantitative rather than qualitative differences (3, 4). HCN4, a pore-forming subunit that is responsible for the pacemaker current I_f, is commonly used to distinguish nodal from chamber myocardium (2). Pacemaking is accomplished by a network of ion channels (M-clock) that act together to generate the pacemaker potential and also involves intracellular Ca^{2+} oscillations (Ca^{2+}-clock) (5–7). Activation of the β-adrenergic receptor leads to the positive chronotropic effect of catecholamines on cardiac automaticity. Enhanced pacemaker activity is believed to involve direct binding of cAMP to HCN channels, but also depends on PKA-dependent phosphorylation of several ion channels that drive the pacemaker potential in sinus node cells (5).

The Popeye domain containing (Popdc) genes encode a family of membrane proteins that are abundantly expressed in heart and skeletal muscle (8–11). In vertebrates, 3 Popdc genes are present: *Popdc1* (previously known as *Pop1*; ref. 9; and also referred to as *Bves*; ref. 8), *Popdc2* (previously known as *Pop2*), and *Popdc3* (previously known as *Pop3*) (8, 9, 12–15). Popdc proteins contain 3 transmembrane helices and the evolutionary conserved cytoplasmic Popeye domain (10, 11). It has been hypothesized that Popdc1 is involved in regulating cell migration, since a loss of *Popdc1* results in early embryonic lethality as a result of defective gastrulation in *Xenopus* and aberrant germ band extension in *Drosophila* (16, 17). In mice, *Popdc1* is required for skeletal muscle regeneration (18). Of the 3 Popdc genes, *Popdc2* shows the highest and most selective expression in myocardium; however, no heart-specific function has been defined for Popdc genes (8–11).

Here, we show that both *Popdc1* and *Popdc2* genes were abundantly expressed in the cardiac pacemaking and conduction system. Mice deficient for either gene developed severe stress-induced cardiac bradycardia in an age-dependent manner. Popdc proteins bound cAMP with high affinity and therefore functioned as mediators in β-adrenergic signal transduction. We also demonstrated that Popdc proteins bound to the 2-pore domain potassium channel TREK-1 and recruited it to the plasma membrane.

Authorship note: Alexander Froese and Stephanie S. Breher are co–first authors. Larissa Fabritz and Thomas Brand are co–senior authors.

Conflict of interest: The authors have declared that no conflict of interest exists.

Citation for this article: *J Clin Invest.* 2012;122(3):1119–1130. doi:10.1172/JCI59410.

This protein interaction was negatively modulated by cAMP. Our present findings led us to conclude that members of the Popdc gene family represent a novel class of cAMP-binding proteins that apparently have a regulatory role in the cardiac pacemaking and conduction system.

Results

To investigate the functional relevance of *Popdc2*, we generated a null mutant mouse by replacing the coding region of exon I by a LacZ reporter gene (Supplemental Figure 1, A–D; supplemental material available online with this article; doi:10.1172/JCI59410DS1). The *Popdc2* null mutant was viable and displayed no obvious pathological phenotype other than reduced weight gain. A cohort of 30 mutant and control littermates was analyzed in the primary systemic screen of the German Mouse Clinic (19), and phenotyping screening data were deposited in the GMC Phenomap database (http://www.mouseclinic.de/phenomap/reports/Popdc2.pdf). Although *Popdc2* is highly expressed in the heart, cardiac morphology and function seemed unaltered in the mutant (Supplemental Figure 1, E–H). Although marker gene expression was increased, no morphological evidence for cardiac hypertrophy was obtained (Supplemental Figure 1, I and J). *Popdc1* and *Popdc3* expression was not elevated in *Popdc2* null mutants (Supplemental Figure 1J).

Popdc2 null mutant mice develop stress-induced bradycardia. *Popdc2* is expressed in cardiac myocytes (20) and showed high levels of expression in the sinus and atrioventricular (AV) nodes (Figure 1, A–D). ECG recordings in freely roaming WT and mutant mice at sedentary state revealed no differences in mean heart rate and rate variability (Supplemental Figure 2A and Supplemental Table 1). In contrast, 5.5- and 8-month-old *Popdc2*$^{-/-}$ animals undergoing physical activity (i.e., swimming exercise) exhibited a mean heart rate that was significantly lower than in WT mice, but was unaltered in 3-month-old mutants (Figure 1, E and F). Similar age-dependent chronotropic incompetence was found when *Popdc2*$^{-/-}$ mice were subjected to mental stress or after direct β-adrenergic stimulation (Supplemental Figure 2B and Supplemental Table 1). Analysis of individual ECG tracings revealed severe sinus node dysfunction (SND) with long pauses and intercurrent periods of normal sinus rhythm (Figure 1G and Supplemental Figure 2C). A sinoatrial block appeared unlikely, since the variation in cycle length at the beginning of a bradycardic period was not a multiple of the preceding cycle length (Supplemental Figure 2D). The number of stress-induced pauses in *Popdc2*$^{-/-}$ mice increased in an age-dependent manner: young adult animals (3 months of age) did not show stress-induced pauses, whereas pauses were common at 8 months of age (Figure 1H). PQ intervals did not differ between genotypes (Figure 1I). Anesthetized mice were subjected to invasive electrophysiological testing of AV node function. The Wenckebach point was not altered in *Popdc2* null mutants (WT, 77.50 ± 5.3, n = 10; *Popdc2*$^{-/-}$, 83.73 ± 3.2, n = 15 per group; P = NS). The AV node in null mutants was able to elicit an escape rhythm during sinus node pauses. We observed narrow and broad-QRS complex escape rhythms in *Popdc2* null mutants (Supplemental Figure 3, D and E), which suggests that the AV node was not functionally impaired. The mutant heart phenotype was not likely due to a defect in autonomic innervation or tone, since isolated, beating, autonomically deprived hearts of *Popdc2*$^{-/-}$ mutants also showed more sinus pauses than did WT littermates during β-adrenergic stimulation (Figure 1J). The drop in mean heart rates after carbachol administration was similar in mutant and WT mice (Supplemental Figure 2E and Supplemental Table 1), indicative of normal responsiveness to parasympathetic stimulation. From these data, we concluded that the *Popdc2*$^{-/-}$ mouse has an intrinsic deficiency to adapt heart rate to physiological stress, which develops in older mice and is mediated at least in part by a blunted heart rate response to catecholamines.

Stress-induced bradycardia is also observed in the Popdc1 null mutant. The presence of a rate-dependent phenotype in *Popdc2* null mutants prompted us to ask whether *Popdc1* deficiency could cause a similar phenotype, although no cardiac pathology has been reported previously (18). *Popdc1*, which is expressed in the heart (18), showed high prevalence in the cardiac pacemaking and conduction system (Figure 2, A–E). Sedentary *Popdc1* null mutant and WT littermate controls showed no difference in mean heart rate and heart rate variability (data not shown). In contrast, after 5 minutes of swimming exercise, the mean heart rate of 8-month-old *Popdc1*$^{-/-}$ mice was lower than that of WT mice (*Popdc1*$^{-/-}$, 593 ± 39 bpm; WT, 701 ± 16 bpm), and severe repetitive drops of the heart rate were observed during and after swim stress (Figure 2F). This abnormality became severe with increasing age in *Popdc1*$^{-/-}$ mice, with significantly more pauses at 5.5 and 8 months of age (Figure 2G). Similar to the *Popdc2* null mutant, heart rate increase in response to mental stress or catecholamines was blunted in *Popdc1*$^{-/-}$ mice (Supplemental Figure 4A) and in isolated, beating *Popdc1*$^{-/-}$ hearts (Supplemental Figure 4B).

Individual ECG recordings of *Popdc1*$^{-/-}$ and WT mice during swim tests revealed severe SND with long pauses interrupting periods of normal sinus rhythm (Figure 2H). The increase of stress-induced pauses in *Popdc1*$^{-/-}$ mice at 8 months of age was striking and amounted to an average of 581 ± 300 pauses during a 30-minute interval after physical exercise compared with 4 ± 2 pauses in WT mice (Figure 2I). The PQ intervals were comparable between the genotypes (Figure 2J). Escape rhythms showed both narrow and broad QRS complexes (Supplemental Figure 3, A–C), consistent with a normal AV nodal automaticity in *Popdc1*$^{-/-}$ mice.

Abnormalities in sinus node structure in Popdc1 and Popdc2 null mutants. In order to search for a structural basis of the bradycardia phenotype in Popdc null mutants, sinus node preparations of 8-month-old *Popdc2*$^{-/-}$ animals were whole-mount stained using an antibody directed against HCN4 (2). The sinus node in WT animals revealed a complex network of nodal myocytes having thin cellular extensions (Figure 3, A, C, and E). In contrast, pacemaker cells in *Popdc2* null mutants displayed a reduced number of these extensions, and the node had a more compact structure (Figure 3, B, D, and F). 3D reconstructions of consecutive Hcn4-stained sections indicated a loss of pacemaker tissue from the inferior part of the sinus node (Figures 3, G and H). Individual sections stained with Trichrome or HCN4 antibody also revealed tissue loss in the inferior sinus node and a compact structure of the superior sinus node in *Popdc2* null mutants (Figure 3, I–P, and Supplemental Figure 5, E–H). We wondered whether the compact superior sinus node was the result of a phenotypic conversion of pacemaker myocytes into working myocardium; however, Cx43, a marker for chamber myocardium, was not ectopically expressed in *Popdc2*$^{-/-}$ mutants (Supplemental Figure 5, A–D). Sinus node preparations of 3-month-old *Popdc2*$^{-/-}$ mutants were indistinguishable from WT preparations (data not shown), which suggests that these histological alterations are only present at an

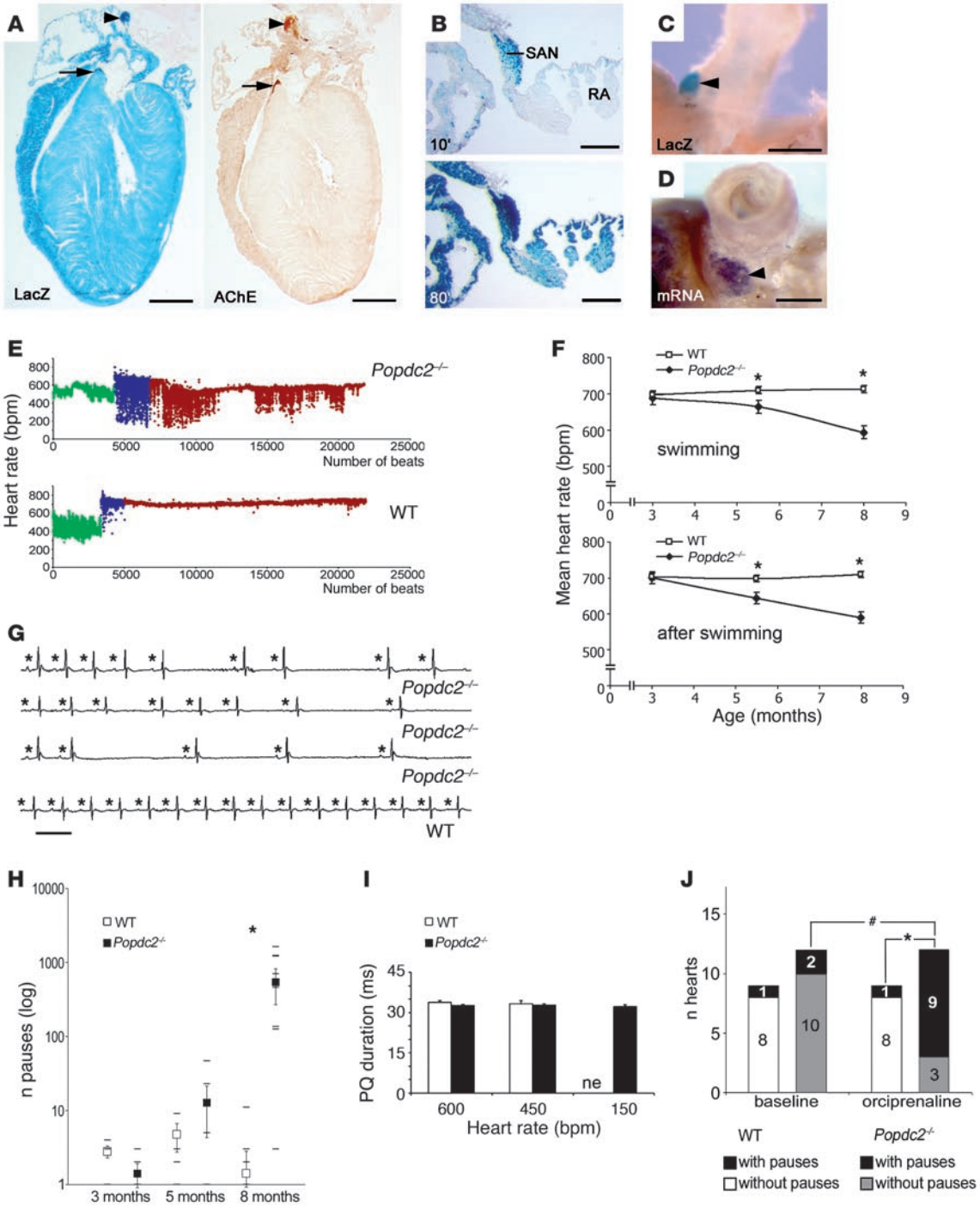

Figure 1

Popdc2$^{-/-}$ mice develop a stress-induced bradycardia. (**A**) Consecutive sections of a *Popdc2*$^{+/-}$ mouse heart were stained for β-galactosidase (LacZ) and acetylcholine esterase (AChE). (**B**) A section through the vena cava region was LacZ stained for 10 or 80 minutes. (**C**) Whole-mount LacZ staining and (**D**) in situ hybridization for *Popdc2*. Arrowheads and arrows in **A**, **C**, and **D** denote sinus and AV nodes, respectively. RA, right atrium; SAN, sinus node. Scale bars: 1 mm (**A**); 200 μm (**B**); 500 μm (**C** and **D**). (**E**) Heart rate distribution (*y* axis) of 8-month-old *Popdc2*$^{-/-}$ and WT mice before (green), during (blue), and after (red) swim stress, depicted on a beat per beat basis (*x* axis). (**F**) Age-dependent mean heart rates of WT and *Popdc2*$^{-/-}$ mice during and after swimming. $^{*}P < 0.05$ between genotypes (n = 5–12). (**G**) ECG recordings of 8-month-old *Popdc2*$^{-/-}$ and WT mice during swim stress test. Asterisks indicate P waves. Horizontal bar: 100 ms. (**H**) Number of pauses in WT and *Popdc2*$^{-/-}$ mice during a 30-minute period after swim stress (log scale on *y* axis) as a function of age (*x* axis). $^{*}P < 0.05$ between genotypes (n = 5–12). (**I**) PQ intervals measured at 600, 450, and 150 bpm (n = 5 per genotype and heart rate). ne, nonexistent in WT. (**J**) Number of isolated hearts with sinus pauses after β-adrenergic stimulation. $^{*}P < 0.05$ between genotypes; $^{\#}P < 0.05$, baseline vs. catecholamine.

age when the mutant displays pacemaker dysfunction. The loss of sinus node tissue may be responsible for the observed phenotype, since the primary pacemaker is known to shift from the center of the sinus node under resting conditions to the inferior part after adrenergic stimulation (21). Therefore, loss of tissue in this part of the sinus node may impair pacemaker activity, especially after adrenergic stimulation. However, it is equally likely that atrophy of the inferior sinus node may be the result of its dysfunction. Interestingly, very similar alterations of sinus node structure were observed in *Popdc1* null animals (Supplemental Figure 6, A–F).

The Popeye domain functions as a high-affinity cAMP-binding domain. The Popeye domain represents a highly conserved structural feature of all Popdc proteins, yet its biochemical function is unknown. Secondary structure predictions of the Popeye domain revealed similarity to the cyclic nucleotide-binding domain of PKA (Figure 4A). However, the amino acid sequence of the putative phosphate-binding cassette (PBC) did not resemble that of other PBC sequences. We directly tested the ability of Popdc proteins to interact with cyclic nucleotides. Binding of native Popdc1 protein to cAMP was demonstrated through affinity precipitation (Figure 4B). Addition of free cAMP to bound Popdc1 protein resulted in a concentration-dependent elution from cAMP-agarose beads, demonstrating specificity of ligand binding. Binding of cAMP was established for all 3 members of the Popdc family (Figure 4C). Sequence alignment of Popeye domains from invertebrates and vertebrates revealed 25 invariant amino acids (data not shown), and 3D modeling allowed us to position most of these conserved residues within or near the putative PBC in the Popeye domain (Figure 4D). According to this model, 2 conserved sequence motifs (DSPE and FQVT) were predicted to be involved in cyclic nucleotide binding (Figure 4E). In order to test this prediction experimentally, we created point mutations in Popdc1 by exchanging the residues D200, P202, and E203 of the DSPE motif to alanine and residue V217 of the FQVT motif to phenylalanine. Popdc1^{D200A} displayed cAMP-binding activity of less than 10% of WT protein, whereas the binding capacity of Popdc1^{P202A} was unchanged (Figure 4F). Popdc1^{E203A} and Popdc1^{V217A} exhibited intermediate binding. A charged-to-alanine mutation of D184 in Popdc2 (which is analogous to D200 in Popdc1) also displayed a substantial reduction in cAMP binding (Figure 4G). To rule out that binding of Popdc proteins to cAMP-agarose is indirectly mediated by an interacting protein, we used a recombinant form of the Popeye domain in a radioimmunoassay. This protein was able to bind to cAMP with high affinity and specificity (cAMP IC_{50}, 118.4 ± 7.1 nM; cGMP IC_{50}, 5.27 ± 0.68 μM; Figure 4H).

Popdc proteins enhance surface expression of the 2-pore domain potassium channel TREK-1. The membrane localization of Popdc1 and Popdc2 in cardiac myocytes (22), the high expression level in cardiac pacemaking tissue, and the heart rate–dependent phenotypes in null mutants suggest an electrical function of Popdc proteins. The I_f current is an essential part of the network of ion channels that act together to generate the pacemaker potential. We tested I_f current density and activation time in isolated sinus node myocytes from WT and *Popdc2*$^{-/-}$ mice. Cells of both genotypes were indistinguishable in current density under basal conditions and after superfusion with 8-Br-cAMP (Supplemental Figure 7A). Moreover, activation kinetics of sinus node cells from WT and *Popdc2*$^{-/-}$ mice were also similar (Supplemental Figure 7B). Therefore, pacemaker dysfunction in *Popdc2*$^{-/-}$ mice was not due to a primary dysfunction of I_f in sinus node cells. We also examined whether Popdc proteins might function as pore-forming units, but did not observe any change in currents in *Xenopus* oocytes after injection of Popdc cRNAs (data not shown). Cardiac myocytes are known to express several 2-pore domain potassium channels, including the stretch-activated K^+ channel TREK-1 and the acid-sensitive K^+ channel TASK-1 (23–25). We analyzed whether the gating properties of these channels might be affected by Popdc proteins. Coexpression of TASK-1 with either Popdc1 or Popdc2 did not alter conductivity (Figure 5A and data not shown). In contrast, coexpression of TREK-1 together with Popdc1, Popdc2, or Popdc3 resulted in a significant augmentation of the outward current measured at +30 mV (Figure 5, B and C). After treating oocytes with theophylline to chronically increase cAMP levels, the relative increase in TREK-1 current was abolished (Figure 5D). The increase in membrane current was likely the result of enhanced expression of TREK-1 at the cell surface, as revealed by a luminometric assay with HA epitope–tagged TREK-1 (Figure 5E). In order to obtain further evidence for a direct interaction between TREK-1 and members of the Popdc family, protein localization was studied in transfected Cos-7 cells. In cells transfected with Popdc1 alone, the protein was localized in the cytoplasm and at the plasma membrane (Figure 5F). In contrast, protein localization of TREK-1 alone was mainly present at the plasma membrane, where it induced filopodia formation, as reported previously (26). When both proteins were expressed simultaneously, they colocalized extensively at the plasma membrane (Figure 5G), which suggests that they form complexes. Interaction of both proteins was also demonstrated in GST pulldown experiments (Figure 5H). Popdc1 also showed substantial coexpression with TREK-1 in isolated adult ventricular cardiac myocytes and in cardiac tissues (Supplemental Figures 8 and 9).

The interaction of Popdc proteins with TREK-1 is modulated by cAMP. The ability of Popdc1 to directly interact with TREK-1 was used to analyze whether cAMP binding might affect complex formation of Popdc1 and TREK-1. For this experiment, we used a bimolecular fluorescence resonance energy transfer (FRET) sensor (Figure 6A). Upon coexpression of cyan fluorescent protein–tagged Popdc1 (Popdc1-CFP) and yellow fluorescent protein–tagged TREK-1 (YFP–TREK-1) in 293A cells, a robust FRET signal confirmed that both proteins interacted directly (Figure 6B). Addition of isoproterenol or forskolin to stimulate cAMP production in these cells resulted in a rapid decline of the YFP/CFP ratio, with the characteristic kinetic of an adenylyl cyclase–dependent process (Figure 6, B, D, and F). Notably, isoproterenol failed to change the FRET signal when the cAMP binding–deficient Popdc1^{D200A} mutant protein was tested (Figure 6, C and F). The addition of sodium nitroprusside to stimulate cGMP production revealed that physiological concentrations of cGMP did not affect the FRET signal (Figure 6, E and F). The cAMP-mediated modulation of the Popdc1–TREK-1 interaction appeared to be a direct allosteric effect of binding, since it was not altered by the PKA inhibitor H89 (Figure 6F). Quantification of the cAMP concentration in cells after isoproterenol treatment using the Epac1-camps sensor for cAMP level calibration (27) established a cAMP/Popdc1 EC_{50} of approximately 330 nM (Figure 6, G and H), which is in agreement with the affinity data obtained by the radioligand binding assay (Figure 4H).

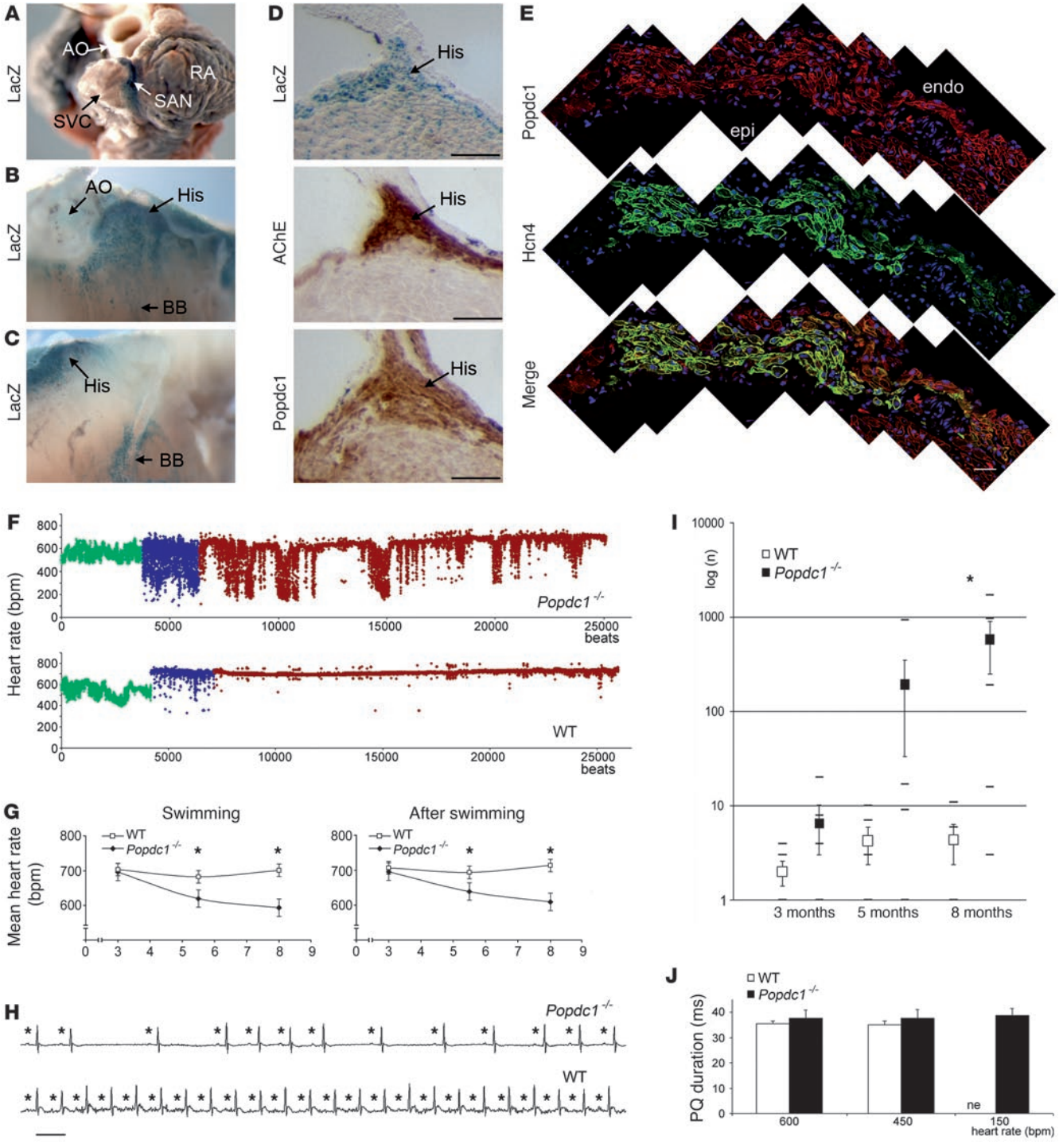

Figure 2

Functional deficits in *Popdc1*$^{-/-}$ mice. (**A**–**C**) Whole-mount LacZ staining of (**A**) sinus node, (**B** and **C**) His bundle (His), and (**B**) left and (**C**) right bundle branches (BB). Ao, aorta; SVC, superior vena cava. (**D**) Consecutive sections through the His bundle were stained for LacZ, acetylcholine esterase, and Popdc1. (**E**) Immunofluorescent detection of Popdc1 and HCN4 and merged images in the sinus node. Shown are composites of multiple images. endo, endocardial; epi, epicardial. Scale bars: 100 μm. (**F**) Heart rate (*y* axis) of *Popdc1*$^{-/-}$ and WT mice before (green), during (blue), and after (red) swim stress, depicted on a beat per beat basis (*x* axis). (**G**) Age-dependent mean heart rates of WT and *Popdc1*$^{-/-}$ mice during and directly after swimming. Shown are mean heart rates (*y* axes) as a function of age (*x* axes). **P* < 0.05 between genotypes (*n* = 5–12). (**H**) ECG recordings of *Popdc1*$^{-/-}$ and WT mice during swim stress test. Asterisks indicate P waves. Horizontal bar: 100 ms. (**I**) Number of pauses in WT and *Popdc1*$^{-/-}$ mice during a 30-minute period after swim stress (log scale on *y* axis) as a function of age (*x* axis). **P* < 0.05 between genotypes (*n* = 5–12). (**J**) PQ intervals measured at 600, 450, and 150 bpm (*n* = 5 per genotype and heart rate).

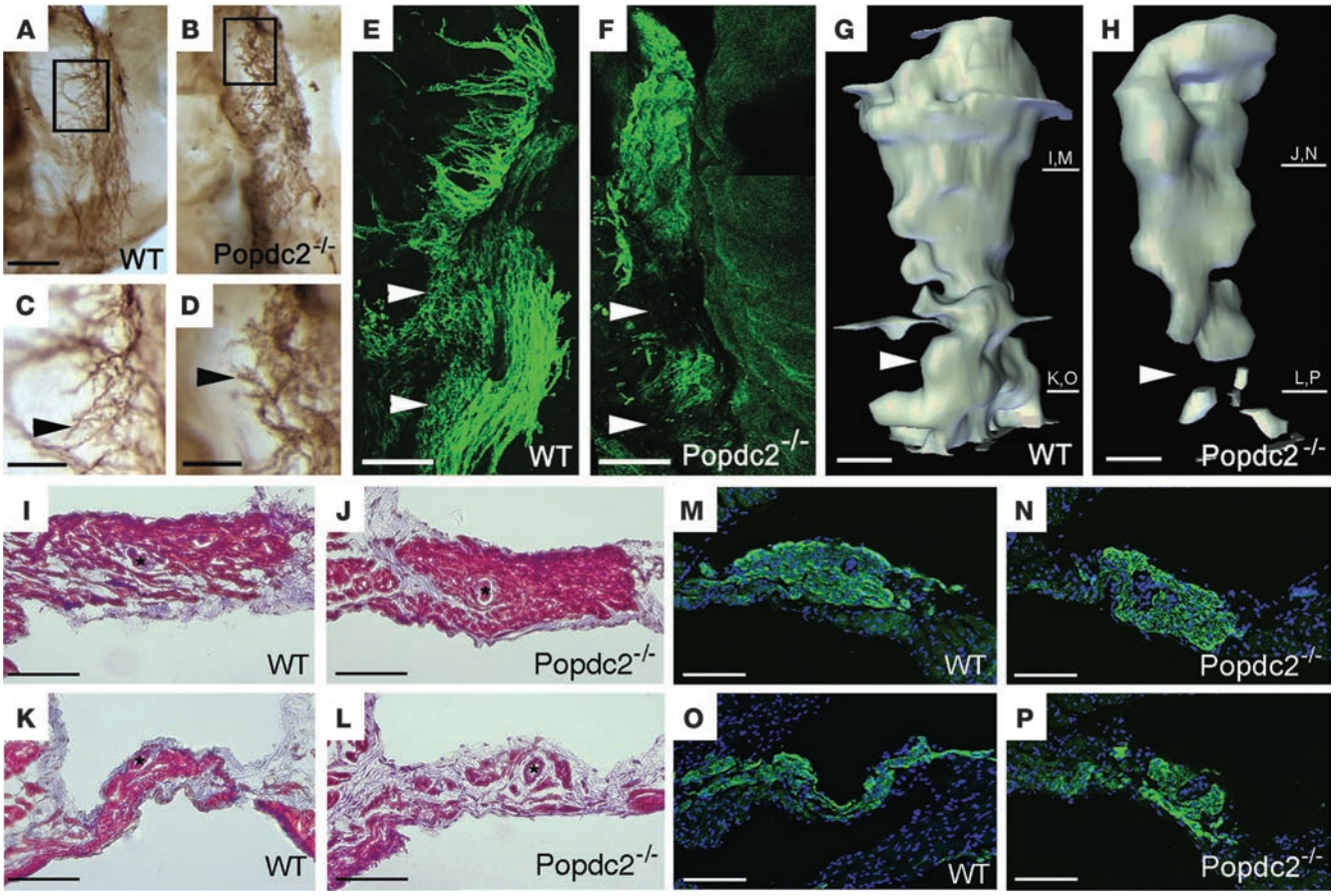

Figure 3
Structural alterations of the sinus node in *Popdc2*$^{-/-}$ mice. (**A**–**D**) Whole-mount immunohistochemistry of HCN4 expression in the sinus node. Boxed regions in **A** and **B** are enlarged in **C** and **D**, respectively. Arrowheads in **C** and **D** denote the network of filopodia-like extensions of nodal myocytes that were structurally abnormal in *Popdc2*$^{-/-}$ mice. (**E** and **F**) Whole-mount immunofluorescence staining of HCN4 in the sinus node illustrating an overall reduction of pacemaking cells in *Popdc2*$^{-/-}$ mice. (**G** and **H**) 3D reconstruction of the sinus node based on HCN4 expression. Arrowheads in **E**–**H** indicate reduction of HCN4 immunoreactivity in the inferior part of the sinus node in mutant mice. Bars at right denote approximate planes of sections shown in **I**–**P**. (**I**–**L**) Trichrome staining visualizing the histology and fibrotic tissue content in the superior (**I** and **J**) and inferior (**K** and **L**) region of the sinus node. (**M**–**P**) Immunohistochemistry for HCN4 expression in the superior (**M** and **N**) and inferior (**O** and **P**) part of the sinus node. Scale bars: 200 μm (**A** and **B**); 100 μm (**C**–**P**).

Discussion

In this report, we demonstrated that loss of function mutations in *Popdc1* and *Popdc2* genes in mice are associated with stress-induced SND, resulting in chronotropic incompetence and long sinus pauses. The Popdc genes displayed overlapping myocardial expression patterns and similar biochemical properties, and the cardiac phenotypes of the null mutants were nearly identical. Our data suggest that Popdc proteins represent a novel class of cAMP binding proteins that interact with TREK-1 channels and may be involved in channel trafficking.

Age-dependent decline in cardiac pacemaking in Popdc null mutants. Both mouse mutants developed SND at advanced age. Assuming that Popdc genes act in the same pathway, loss of a single gene might not have a significant impact on function in the young, since both Popdc genes might be able to substitute for each other. Obviously, the compensation became less efficient when the null mutants aged, possibly due to an age-dependent decline of Popdc expression. Alternatively, the concentration of essential interacting proteins might become limiting. Preliminary electrophysiological analysis of double homozygous *Popdc1/Popdc2* mutant mice lends support to the hypothesis of functional redundancy. Double null animals displayed decreased tolerance to stress and frequently underwent sudden cardiac death under stress conditions. This is consistent with an augmented heart phenotype when both Popdc genes are absent.

Cardiac pacemaking depends on spontaneous sarcoplasmic reticulum Ca^{2+} cycling, which is driven by cAMP-mediated, PKA-dependent phosphorylation and interacts with a network of plasma membrane localized ion channels (7). At present, it is unclear how Popdc proteins might fit into this intricate network, but it is likely that an abundantly expressed and membrane localized cAMP-binding protein could have an important role in cAMP signaling and/or compartmentalization in cardiac myocytes. It is tempting to speculate that cAMP binding to Popdc proteins modulates the function of pacemaker currents. Therefore, it will be important to study the impact of age on

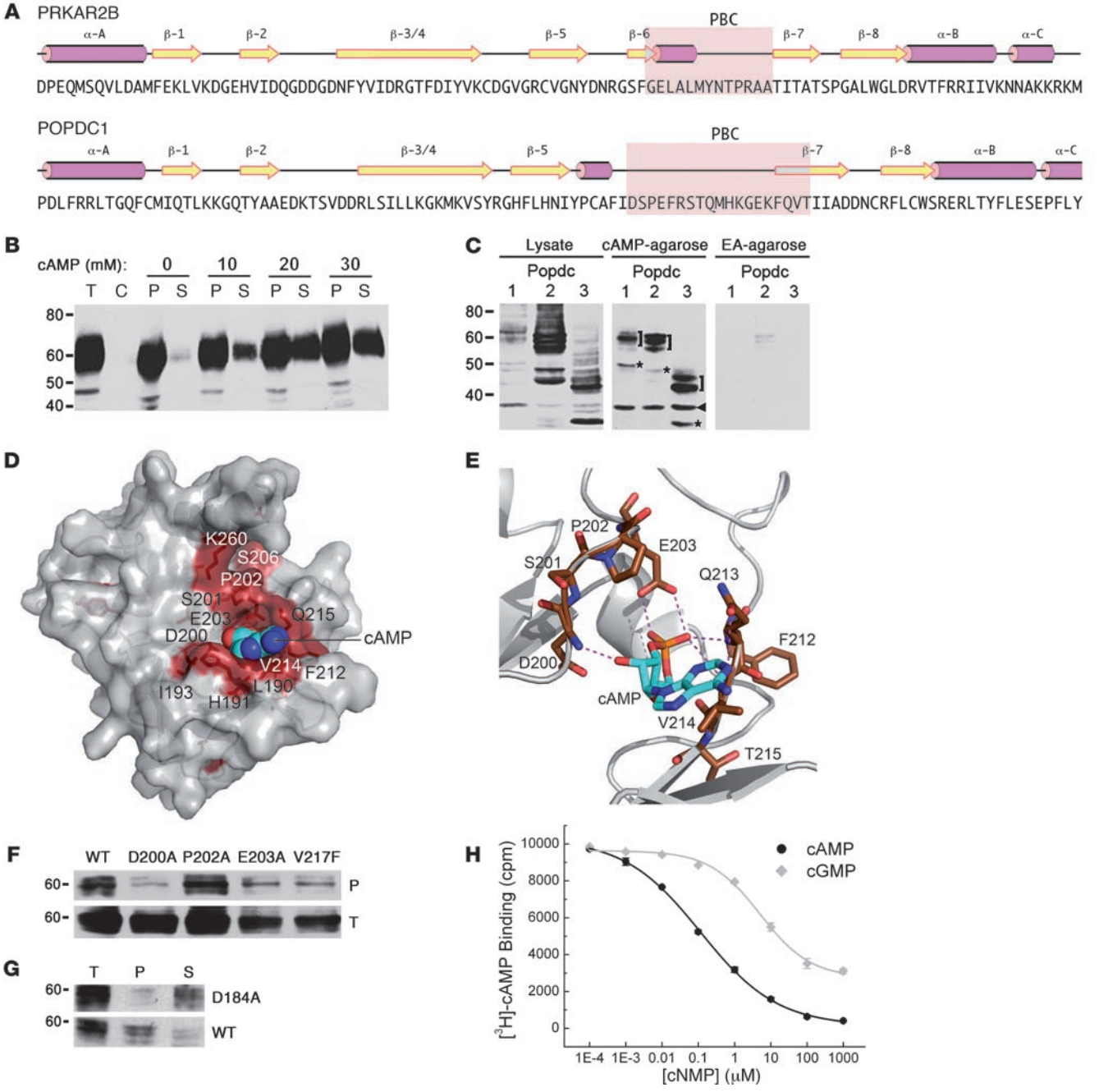

Figure 4

The Popeye domain functions as a cyclic nucleotide-binding domain. (**A**) Secondary structure of human cAMP-dependent protein kinase type II-β regulatory subunit (PRKAR2B) and structural prediction of the Popeye domain of human POPDC1. Pink rods, α helices; yellow arrows, β strands; pink underlay, PBC. (**B**) Western blot detection of chick Popdc1 after affinity precipitation of cardiac tissue extracts incubated with cAMP-agarose. Bound Popdc1 protein was eluted with increasing amounts of cAMP. P, pellet; S, supernatant; T, total protein; C, control incubation using ethanolamine-agarose. (**C**) Western blot of Cos-7 cells transfected with Popdc1, Popdc2, and Popdc3 cDNAs. Shown are total protein and protein bound to cAMP-agarose or ethanolamine (EA) agarose. Brackets denote differentially glycosylated Popdc proteins; asterisks denote nonglycosylated form of Popdc proteins; arrowhead denotes unspecific immunoreactive protein. (**D**) 3D model of the Popeye domain of human POPDC1. Invariant amino acids are colored red. The cAMP moiety is shown as CPK model. (**E**) Enlargement of the predicted cAMP binding site. Predicted hydrogen bonds between cAMP and the DSPE and FQVT sequence motifs are shown as dashed lines. (**F**) Western blot of cAMP-agarose precipitations of Cos-7 cells transfected with cDNAs encoding Popdc1 and Popdc1^{D200A}, Popdc1^{P202A}, Popdc1^{E203A}, or Popdc1^{V217F} mutants. (**G**) Western blot of cAMP-agarose precipitations of Cos-7 cells transfected with cDNAs encoding Popdc2 or Popdc2^{D184A} mutant. (**H**) Radioligand binding assay using [^{3}H]-cAMP and recombinant C terminus of Popdc1. Binding was competed with increasing concentrations of free unlabeled cAMP and cGMP, respectively.

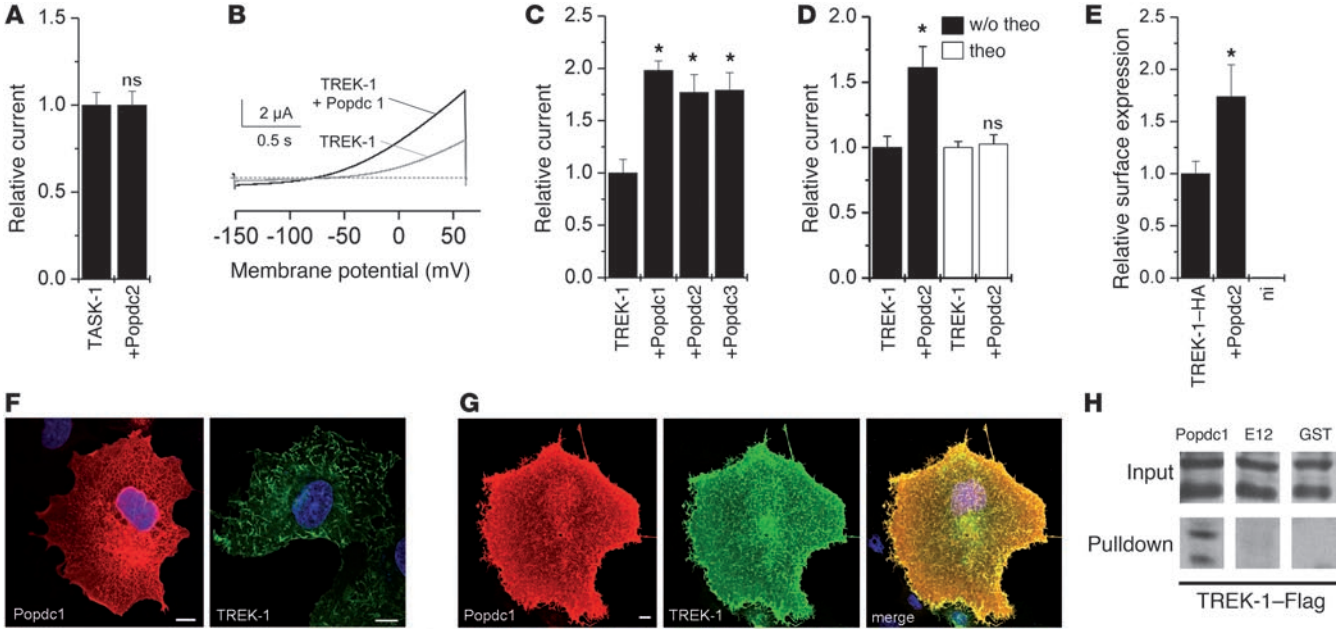

Figure 5

Interaction of Popdc proteins with the 2-pore channel TREK-1. (**A**) Relative current amplitudes of TASK-1 alone or in the presence of Popdc2 were assayed in *Xenopus* oocytes 48–72 hours after injection (n = 28–31). Error bars in **A** and **C**–**E** are SEM. (**B**) Example of the measurement of TREK-1–mediated outward current after injection of TREK-1 cRNA alone (gray curve) or in the presence of Popdc1 (black curve) in *Xenopus* oocytes. (**C**) Relative current amplitudes of TREK-1 alone or in the presence of Popdc1, Popdc2, or Popdc3 (n = 14–22). *P < 0.05. (**D**) Relative TREK-1 current amplitudes in the presence or absence of Popdc2. The oocytes were incubated for 48 hours with or without theophylline (n = 17–32). *P < 0.05. (**E**) Quantification of the relative surface expression of HA-tagged rat TREK-1b in the presence or absence of mouse Popdc2 (n = 27 and 19, respectively). ni, noninjected control oocytes (n = 12). *P < 0.05. (**F** and **G**) Immunostaining of Popdc1 (red) or TREK-1 (green) transfected individually (**F**) or both together (**G**) into Cos-7 cells. Nuclei were counterstained with DAPI. Scale bars: 10 μm. (**H**) Example of a GST pulldown experiment using the C terminus of Popdc1 fused to GST and Flag-tagged human TREK-1. GST-E12 and GST proteins were used as controls.

cAMP levels in sinus node cells and the downstream signaling cascades of cAMP in response to β-adrenergic receptor stimulation (28, 29). Of note, older sinus node myocytes show a blunted chronotropic response after phosphodiesterase inhibition (30). Moreover, an age-associated decline in Ca^{2+} cycling occurs in ventricular myocytes and in sinus node cells (31). Thus, in the Popdc null mutants, the loss of a potential mediator of cAMP signaling may be further exacerbated by an age-dependent decline in cAMP signaling. This may explain why only a stress-induced phenotype was observed.

SND in humans is a disease of unknown etiology. It is often associated with a loss of pacemaker tissue, increased fibrosis, and a growing distance between the sinus node and working myocardium (32). While the disease is heterogeneous, there is a strong association with age. Moreover, in a substantial number of cases, a genetic basis seems likely, and point mutations in genes encoding ion channels and proteins involved in channel trafficking have been associated with SND (33–36). Our observation that both Popdc null mutants had SND suggests that these genes may be candidate genes for this disease and that mutations might be found in familial cases. Moreover, the mouse mutants can be considered suitable models for studying the etiology of SND and possible therapies.

Interaction of Popdc proteins with TREK-1. Increasing evidence points to the fact that ion channels act in the context of macromolecular signaling complexes, consisting of pore-forming subunits in association with auxiliary subunits, regulatory enzymes, and proteins that are involved in membrane targeting and complex formation (37). Cardiac arrhythmias are associated with mutations in genes encoding ion channels as well as proteins involved in targeting channels to the membrane or acting as β subunits (38). In *Xenopus* oocytes, we found a strong correlation between the ability of Popdc protein to enhance TREK-1 current and the recruitment of TREK-1 channels to the plasma membrane. Thus, Popdc proteins are potentially acting on TREK-1 channel trafficking.

In neuronal cells, TREK-1 has previously been shown to play an essential role as a background K^+ channel, setting the resting membrane potential and modulating action potentials (39). Although TREK-1 is expressed in the heart, together with other related 2-pore domain channels, its role — particularly in pacemaking — has not yet been established (40). Interestingly, ORK1, a TREK-1 ortholog in *Drosophila*, performs essential pacemaking functions in the fly heart (41). It is tempting to hypothesize that direct binding of cAMP to Popdc proteins in a complex with TREK-1 at the plasma membrane provides a mechanism by which adrenergic stimulation regulates TREK-1 gating. This would be a novel mode of modulation that works in addition to the well-established inhibition of TREK-1 through direct phosphorylation by PKA (23, 42). In this regard, our bimolecular

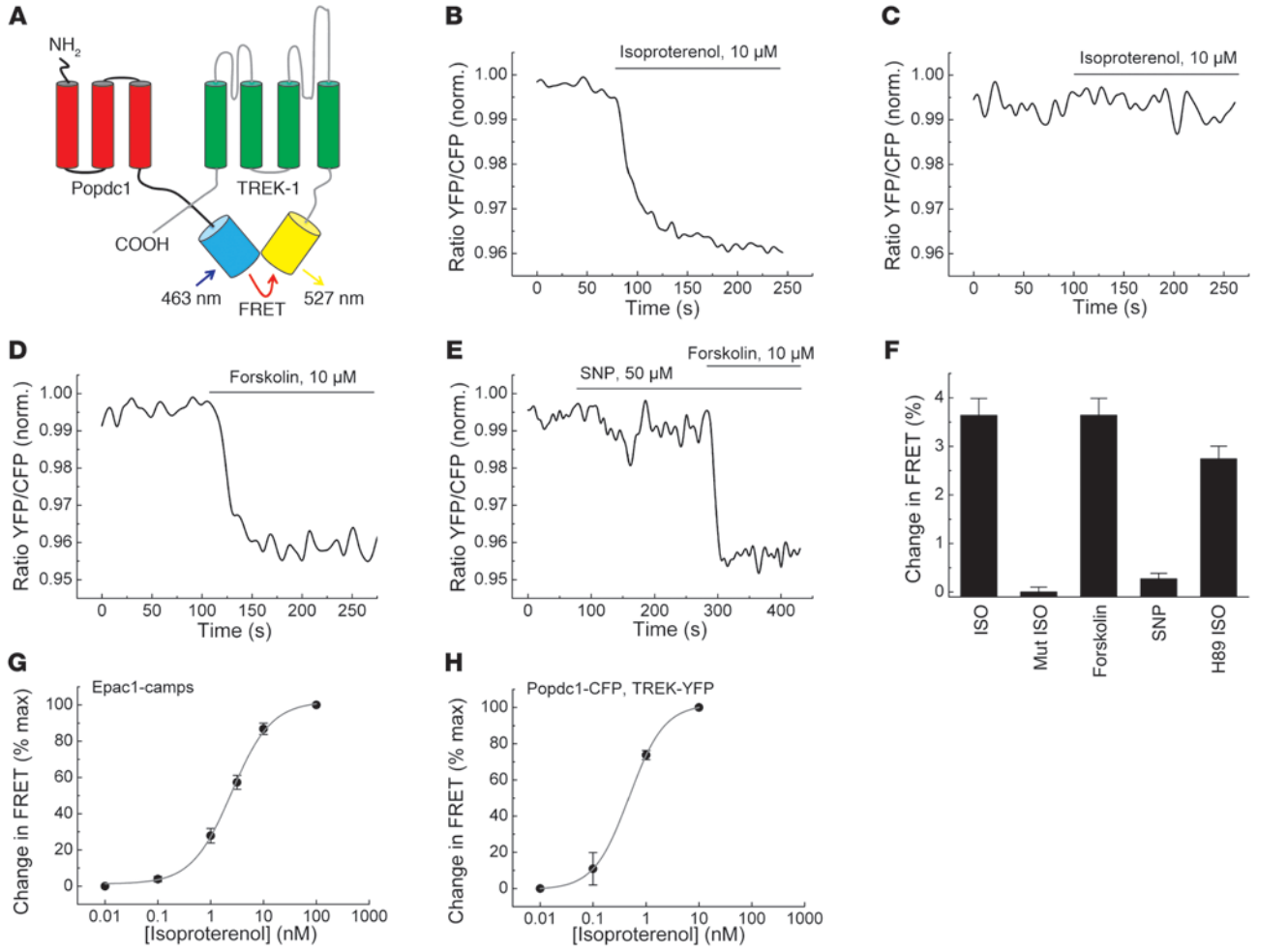

Figure 6

The interaction of Popdc1 and TREK-1 is modulated by cAMP. (**A**) Schematic depiction of the bimolecular FRET sensor to study the interaction of Popdc1 and TREK-1. (**B**–**E**) FRET measurements of 293A cells transfected with YFP–TREK-1 together with Popdc1-CFP (**B**, **D**, and **E**) or Popdc1^{D200A}-CFP (**C**). Cells were stimulated with isoproterenol (**B** and **C**), forskolin (**D**), or sodium nitroprusside (SNP) followed by the addition of forskolin (**E**). Values are normalized YFP/CFP ratios. (**F**) Summary of the observed relative changes of FRET signals (mean ± SEM). ISO, isoproterenol; Mut ISO, Popdc1^{D200A}-CFP treated with isoproterenol; H89 ISO, addition of PKA inhibitor H89 and isoproterenol. (**G** and **H**) Concentration-dependent response curve for isoproterenol-induced FRET signals using Epac1-camps (**G**) or Popdc1-CFP/YFP–TREK-1 (**H**).

FRET data supported a direct modulatory role of cAMP, which affected the interaction of TREK-1 and Popdc proteins. In *Xenopus* oocytes, Popdc1 affected membrane trafficking of TREK-1. Experiments in cardiac myocytes will be needed to further study how Popdc proteins affect TREK-1 activity, in particular after adrenergic stimulation. It will also be important to assess whether cardiac pacemaker function is altered in the TREK-1 null mutant (43).

TREK-1 induces filopodia formation through interaction with the actin cytoskeleton (26), and after cotransfection, Popdc1 was also present in these membrane protrusions, which suggests that TREK-1 and Popdc1 might be part of the same macromolecular complex. TREK-1 is known to interact with AKAP150, a PKA anchor protein, as well as Mtap2, a microtubule-associated protein (44–46). Mtap2 enhances TREK-1 current by recruiting channel proteins to the plasma membrane. On the other hand, AKAP150 interaction with TREK-1 enhances gating, but also modifies the channel properties. It has also been shown that the coexpression of both interacting proteins provides additive effects on TREK-1 current (44–46). Thus, it will be interesting to study the modulation of TREK-1 current in the presence of Popdc proteins and these other TREK-1 interaction partners.

It is likely that, in addition to TREK-1, other interacting proteins are contributing to the bradycardia phenotype. This assumption is based on the abundance of Popdc proteins. In particular, Popdc2 was highly expressed in cardiac myocytes, and therefore probably will have other interaction partners in addition to TREK-1. These proteins could contribute to the stress-induced bradycardia phenotype. We are currently screening for such Popdc-interacting proteins using several independent approaches. Apart from ion channels and pumps, it is pos-

sible that Popdc also interacts with proteins involved in channel oligomerization or membrane trafficking. VAMP2/3 and GEFT are 2 proteins that have been shown to interact with Popdc1 (47, 48). VAMP2/3 has been shown to be involved in membrane vesicle fusion and could be involved in ion channel trafficking. GEFT, on the other hand, is a regulator of RhoA, and this interaction may be responsible for the cell shape changes that were observed in the sinus node of Popdc null mutants. However, it is not presently known whether Popdc2 is also interacting with VAMP2/3 and GEFT.

Popdc proteins represent a class of cAMP-binding proteins that we believe to be novel. Despite the importance of cAMP as a second messenger molecule involved in numerous physiological regulatory modules, only a limited number of effector proteins are known to date (49). The most important effector is PKA, which is responsible for many of the molecular changes that occur in response to rising levels of cAMP. In addition to PKA, Epac proteins couple intracellular cAMP to the activation of Rap1, a Ras family GTPase that regulates cell adhesion, proliferation, and differentiation (50). Thus, structural changes in response to an elevation in cAMP levels are probably regulated to a large extent by EPAC proteins. Several ion channels also directly bind cyclic nucleotides, which modulates the activation characteristics or gating properties of these channels; therefore, cAMP regulates membrane potential and excitability of cells. Although HCN4 plays an important role in cardiac pacemaker function (51, 52), despite its ability to directly bind cAMP, its role in stress adaptation of the cardiac pacemaker remains a matter of debate (51, 53–55). Therefore, our present identification of Popdc proteins as a class of membrane-localized cAMP binding proteins in sinus node cells and our finding that genetic loss resulted in stress-induced bradycardia suggest that Popdc proteins are part of the molecular network involved in cardiac pacemaker regulation in response to adrenergic stimulation. We believe the Popeye domain represents a novel class of cAMP-binding domain, and its PBC is highly divergent from that of other cAMP effector proteins (56, 57). This sequence divergence provides the opportunity to develop novel pharmacological agents to specifically target Popdc function and to study its role in health and disease.

Methods

Further information can be found in Supplemental Methods.

Mice. The *Popdc2* null mutant was engineered by replacing the coding sequence of the first exon with the LacZ reporter gene (Supplemental Figure 1). The *Popdc1* null mutant mouse was described previously (18).

ECG. To assess cardiac size, morphology, and function, 2-dimensional echocardiography and Doppler measurements were performed using 13.5-MHz 2 D and M Mode and 12-MHz Doppler transducers (HP Sonos) and a small animal ultrasound platform (VEVO770) equipped with a 50-MHz transducer following published protocols (58, 59).

ECG and telemetry. ECGs in freely roaming animals were recorded in littermate pairs at 3, 5.5, and 8 month of age. The telemetric ECG was analyzed during normal activity and during defined stress tests, i.e., swimming, air jets, or isoproterenol (60, 61). Surface ECG data at baseline and after isoproterenol stimulation (2 mg/kg body weight) were obtained in anesthetized animals. For invasive electrophysiological testing, an octapolar 2-French catheter was used. Incremental atrial pacing was performed until the first impulse was blocked in the AV node (Wenckebach point).

Electrophysiological study in the isolated heart. Intrinsic heart rate and pauses were recorded at baseline and during perfusion with 1.6 μM orciprenaline in Langendorff-perfused hearts (60, 61).

Enzyme histochemistry. β-Galactosidase and acetylcholinesterase stainings were performed as described previously (20, 62).

Whole-mount in situ hybridization. The inflow tract of an adult heart was subjected to whole-mount in situ hybridization using a Popdc2 cRNA probe as described elsewhere (63).

PCR analysis. qPCR was performed using SYBR Green. See Supplemental Methods for details and primer sequences.

Mutagenesis. Popdc1^{D200A}, Popdc1^{P202A}, Popdc1^{E203A}, Popdc1^{V217F}, and Popdc2^{D184A} were generated by site-directed mutagenesis using the QuikChange Site-Directed Mutagenesis Kit (Stratagene). See Supplemental Methods for details and primer sequences.

cAMP affinity precipitation. Lysates of transfected cells or dissected tissues were incubated with cAMP-agarose. Binding was competed with varying concentrations of free cAMP. Bound protein was detected by Western blot analysis.

Surface expression analysis. Surface expression of HA-tagged TREK-1 in the presence or absence of Popdc2 was quantitated by an immunoluminometric assay as described previously (64).

GST pulldown. Cell lysate of Cos-7 cells transiently transfected with TREK-1–Flag was added to GST-Bves, GST-E12, or GST protein bound to glutathione-sepharose 4B beads. Bound protein was detected by Western blot analysis.

Western blot analysis. Protein samples were run on SDS-PAGE and immunoblotted with the following antibodies: α-chick Popdc1 (Pop1 3F11; ref. 65), α-mouse Popdc1 (BVES C-20; Santa Cruz), α-Myc (9E10; Abcam), α-FLAG (M2; Sigma-Aldrich).

Measurement of TREK-1 current. Human TREK-1c cRNA together with mouse Popdc cRNAs were injected into *Xenopus laevis* oocytes, and 2-electrode voltage-clamp measurements were performed 24–72 hours after injection (25).

Electrophysiology of sinus node myocytes. Single myocytes from the sinus node were isolated and prepared for electrophysiological recordings as described previously (66, 67). I_f was recorded with the whole-cell patch-clamp recording in the presence or absence of 8-Br-cAMP.

Modeling of the Popeye domain. Modeling of the Popeye domain of human POPDC1 was based on the structure of the N-terminal domain of a transcriptional regulator from *Streptomyces coelicolor* (PDB entry 2PQQ) and the cAMP-binding domain of cAMP-dependent protein kinase (PKA; PDB entry 1CX4).

FRET assay. 293A cells were transiently transfected with Popdc1-CFP and YFP–TREK-1 constructs, and FRET measurements were performed 24 hours later using a Zeiss Axiovert 200 inverted microscope.

Radioligand binding assay. Purified GST fusion protein of the C terminus of Popdc1 was incubated with [^{3}H]-cAMP and increasing concentrations of unlabeled cAMP or cGMP, and the bound radioactivity was measured.

Statistics. Paired and unpaired 2-tailed *t* tests, univariate ANOVA, and ANOVA analyses for multiple comparisons and repetitive measurements were used for comparison of continuous parameters at different cycle lengths in WT, *Popdc1*$^{-/-}$, and *Popdc2*$^{-/-}$ mutant mice at baseline and with drugs. Fisher exact test was used to compare hearts with occurrence of sinus pauses. Unless otherwise indicated, values are mean ± SEM. Statistical significance was accepted at a P value less than 0.05.

Study approval. Mouse handling and experimentation were performed following institutional guidelines and were approved by the University of Münster institutional animal care and use committee (protocol nos. G61/99, G83/2004).

Acknowledgments

This work was supported by Deutsche Forschungsgemeinschaft (DFG) grants BR1218/9-4 (to T. Brand) and DE-1482/3-2 (to N. Decher); by Graduate College grants 1048 'Organogenesis' (to T. Brand), SFB 656 A8 (to L. Fabritz and P. Kirchhof), Ki 731 (to P. Kirchhof), and FA 413/3-1 (to L. Fabritz); by the Interdisciplinary Center for Clinical Research (IZKF) Münster Core Unit CarTel (to P. Kirchhof) and grant Kih1/020/07 (to L. Fabritz); and by Fondation Leducq (to P. Kirchhof). We thank Christian Dees, Reinhild Fischer, Elisabeth Meyer-Natus, Nina Kreienkamp, Daniela Volkery, Marco Abesser, Ursula Herbort-Brand, and Marcel Tekook for excellent technical assistance and Lisa Fortmüller for help with the in vivo pathophysiology.

Received for publication June 14, 2011, and accepted in revised form December 21, 2011.

Address correspondence to: Thomas Brand, Harefield Heart Science Centre, National Heart and Lung Institute, Imperial College London, Harefield, UB9 6JH, United Kingdom. Phone: 44.0.1895.453.826; Fax: 44.0.1895.828.900; E-mail: t.brand@imperial.ac.uk.

Alexander Froese and Stephanie S. Breher's present address is: Department of Cardiology and Angiology, Hannover Medical School, Hannover, Germany.

Roland F.R. Schindler, Jan Schlueter, and Thomas Brand's present address is: Heart Science Centre, Imperial College London, Harefield, United Kingdom.

Viacheslav Nikolaev's present address is: Department of Cardiology and Pneumology, University of Göttingen, Göttingen, Germany.

Juliane Khutz's present address is: Institute of Human Genetics, University of Würzburg, Würzburg, Germany.

Patrick Meister's present address is: Developmental Biochemistry, University of Würzburg, Würzburg, Germany.

Sonja Kreissl's present address is: Comprehensive Heart Failure Center (CHFC), University Hospital Würzburg, Würzburg, Germany.

Angela Torlopp's present address is: Cell and Developmental Biology, University College London, London, United Kingdom.

Larissa Fabritz and Paulus Kirchhof's present address is: Centre for Cardiovascular Sciences, University of Birmingham, Birmingham, United Kingdom.

1. Anderson RH, Yanni J, Boyett MR, Chandler NJ, Dobrzynski H. The anatomy of the cardiac conduction system. *Clin Anat*. 2009;22(1):99–113.
2. Liu J, Dobrzynski H, Yanni J, Boyett MR, Lei M. Organisation of the mouse sinoatrial node: structure and expression of HCN channels. *Cardiovasc Res*. 2007;73(4):729–738.
3. Tellez JO, et al. Differential expression of ion channel transcripts in atrial muscle and sinoatrial node in rabbit. *Circ Res*. 2006;99(12):1384–1393.
4. Marionneau C, et al. Specific pattern of ionic channel gene expression associated with pacemaker activity in the mouse heart. *J Physiol*. 2005;562(pt 1):223–234.
5. Mangoni ME, Nargeot J. Genesis and regulation of the heart automaticity. *Physiol Rev*. 2008;88(3):919–982.
6. Noble D, Noble PJ, Fink M. Competing oscillators in cardiac pacemaking: historical background. *Circ Res*. 2010;106(12):1791–1797.
7. Lakatta EG, Maltsev VA, Vinogradova TM. A coupled SYSTEM of intracellular Ca2+ clocks and surface membrane voltage clocks controls the timekeeping mechanism of the heart's pacemaker. *Circ Res*. 2010; 106(4):659–673.
8. Reese DE, Zavaljevski M, Streiff NL, Bader D. bves: A novel gene expressed during coronary blood vessel development. *Dev Biol*. 1999;209(1):159–171.
9. Andrée B, Hillemann T, Kessler-Icekson G, Schmitt-John T, Jockusch H, Arnold HH, Brand T. Isolation and characterization of the novel popeye gene family expressed in skeletal muscle and heart. *Dev Biol*. 2000;223(2):371–382.
10. Brand T. The popeye domain-containing gene family. *Cell Biochem Biophys*. 2005;43(1):95–104.
11. Osler ME, Smith TK, Bader DM. Bves, a member of the Popeye domain-containing gene family. *Dev Dyn*. 2006;235(3):586–593.
12. Hitz MP, Pandur P, Brand T, Kuhl M. Cardiac specific expression of Xenopus Popeye-1. *Mech Dev*. 2002;115(1–2):123–126.
13. Breher SS, Mavridou E, Brenneis C, Froese A, Arnold HH, Brand T. Popeye domain containing gene 2 (Popdc2) is a myocyte-specific differentiation marker during chick heart development. *Dev Dyn*. 2004;229(3):695–702.
14. Torlopp A, Breher SS, Schluter J, Brand T. Comparative analysis of mRNA and protein expression of Popdc1 (Bves) during early development in the chick embryo. *Dev Dyn*. 2006;235(3):691–700.
15. Parnes D, Jacoby V, Sharabi A, Schlesinger H, Brand T, Kessler-Icekson G. The Popdc gene family in the rat: molecular cloning, characterization and expression analysis in the heart and cultured cardiomyocytes. *Biochim Biophys Acta*. 2007;1769(9–10):586–592.
16. Ripley AN, Osler ME, Wright CV, Bader D. Xbves is a regulator of epithelial movement during early Xenopus laevis development. *Proc Natl Acad Sci U S A*. 2006;103(3):614–619.
17. Lin S, Zhao D, Bownes M. Blood vessel/epicardial substance (bves) expression, essential for embryonic development, is down regulated by Grk/EFGR signalling. *Int J Dev Biol*. 2007;51(1):37–44.
18. Andrée B, Fleige A, Arnold HH, Brand T. Mouse Pop1 is required for muscle regeneration in adult skeletal muscle. *Mol Cell Biol*. 2002;22(5):1504–1512.
19. Gailus-Durner V, et al. Introducing the German Mouse Clinic: open access platform for standardized phenotyping. *Nat Methods*. 2005;2(6):403–404.
20. Froese A, Brand T. Expression pattern of Popdc2 during mouse embryogenesis and in the adult. *Dev Dyn*. 2008;237(3):780–787.
21. Opthof T. The mammalian sinoatrial node. *Cardiovasc Drugs Ther*. 1988;1(6):573–597.
22. Smith TK, Bader DM. Characterization of Bves expression during mouse development using newly generated immunoreagents. *Dev Dyn*. 2006; 235(6):1701–1708.
23. Terrenoire C, Lauritzen I, Lesage F, Romey G, Lazdunski M. A TREK-1-like potassium channel in atrial cells inhibited by beta-adrenergic stimulation and activated by volatile anesthetics. *Circ Res*. 2001;89(4):336–342.
24. Xian Tao L, et al. The stretch-activated potassium channel TREK-1 in rat cardiac ventricular muscle. *Cardiovasc Res*. 2006;69(1):86–97.
25. Putzke C, et al. The acid-sensitive potassium channel TASK-1 in rat cardiac muscle. *Cardiovasc Res*. 2007;75(1):59–68.
26. Lauritzen I, et al. Cross-talk between the mechanogated K2P channel TREK-1 and the actin cytoskeleton. *EMBO Rep*. 2005;6(7):642–648.
27. Nikolaev VO, Bunemann M, Hein L, Hannawacker A, Lohse MJ. Novel single chain cAMP sensors for receptor-induced signal propagation. *J Biol Chem*. 2004;279(36):37215–37218.
28. Lakatta EG, Levy D. Arterial and cardiac aging: major shareholders in cardiovascular disease enterprises: Part II: the aging heart in health: links to heart disease. *Circulation*. 2003;107(2):346–354.
29. Lakatta EG. Arterial and cardiac aging: major shareholders in cardiovascular disease enterprises: Part III: cellular and molecular clues to heart and arterial aging. *Circulation*. 2003;107(3):490–497.
30. Sirenko S, Shukla S, Liu J, Lakatta EG. Age associated decrease in intrinsic action potential firing rate in sinoatrial node cells is linked to a deficient intrinsic cAMP-PKA-Ca2+ signaling. *Biophys J*. 2011;100(3):434a.
31. Janczewski AM, Lakatta EG. Modulation of sarcoplasmic reticulum Ca(2+) cycling in systolic and diastolic heart failure associated with aging. *Heart Fail Rev*. 2010;15(5):431–445.
32. Dobrzynski H, Boyett MR, Anderson RH. New insights into pacemaker activity: promoting understanding of sick sinus syndrome. *Circulation*. 2007;115(14):1921–1932.
33. Ruan Y, Liu N, Priori SG. Sodium channel mutations and arrhythmias. *Nat Rev Cardiol*. 2009; 6(5):337–348.
34. Schulze-Bahr E, et al. Pacemaker channel dysfunction in a patient with sinus node disease. *J Clin Invest*. 2003;111(10):1537–1545.
35. Milanesi R, Baruscotti M, Gnecchi-Ruscone T, DiFrancesco D. Familial sinus bradycardia associated with a mutation in the cardiac pacemaker channel. *N Engl J Med*. 2006:354(2):151–157.
36. Tan HL, et al. A sodium-channel mutation causes isolated cardiac conduction disease. *Nature*. 2001;409(6823):1043–1047.
37. Mohler PJ, Wehrens XH. Mechanisms of human arrhythmia syndromes: abnormal cardiac macromolecular interactions. *Physiology (Bethesda)*. 2007;22:342–350.
38. Ackerman MJ, Mohler PJ. Defining a new paradigm for human arrhythmia syndromes: phenotypic manifestations of gene mutations in ion channel- and transporter-associated proteins. *Circ Res*. 2010;107(4):457–465.
39. Honore E. The neuronal background K2P channels: focus on TREK1. *Nat Rev Neurosci*. 2007;8(4):251–261.

40. Gurney A, Manoury B. Two-pore potassium channels in the cardiovascular system. *Eur Biophys J*. 2009;38(3):305–318.
41. Lalevee N, Monier B, Senatore S, Perrin L, Semeriva M. Control of cardiac rhythm by ORK1, a Drosophila two-pore domain potassium channel. *Curr Biol*. 2006;16(15):1502–1508.
42. Patel AJ, et al. A mammalian two pore domain mechano-gated S-like K+ channel. *EMBO J*. 1998; 17(15):4283–4290.
43. Heurteaux C, et al. Deletion of the background potassium channel TREK-1 results in a depression-resistant phenotype. *Nat Neurosci*. 2006;9(9):1134–1141.
44. Bockenhauer D, Zilberberg N, Goldstein SA. KCNK2: reversible conversion of a hippocampal potassium leak into a voltage-dependent channel. *Nat Neurosci*. 2001;4(5):486–491.
45. Sandoz G, et al. AKAP150, a switch to convert mechano-, pH- and arachidonic acid-sensitive TREK K(+) channels into open leak channels. *EMBO J*. 2006;25(24):5864–5872.
46. Sandoz G, Tardy MP, Thummler S, Feliciangeli S, Lazdunski M, Lesage F. Mtap2 is a constituent of the protein network that regulates twik-related K+ channel expression and trafficking. *J Neurosci*. 2008;28(34):8545–8552.
47. Hager HA, Roberts RJ, Cross EE, Proux-Gillardeaux V, Bader DM. Identification of a novel Bves function: regulation of vesicular transport. *EMBO J*. 2010;29(3):532–545.
48. Smith TK, Hager HA, Francis R, Kilkenny DM, Lo CW, Bader DM. Bves directly interacts with GEFT, and controls cell shape and movement through regulation of Rac1/Cdc42 activity. *Proc Natl Acad Sci U S A*. 2008;105(24):8298–8303.
49. Rehmann H, Wittinghofer A, Bos JL. Capturing cyclic nucleotides in action: snapshots from crystallographic studies. *Nat Rev Mol Cell Biol*. 2007;8(1):63–73.
50. Gloerich M, Bos JL. Epac: defining a new mechanism for cAMP action. *Ann Rev Pharmacol Toxicol*. 2010;50:355–375.
51. Baruscotti M, et al. Deep bradycardia and heart block caused by inducible cardiac-specific knockout of the pacemaker channel gene Hcn4. *Proc Natl Acad Sci U S A*. 2011;108(4):1705–1710.
52. Stieber J, et al. The hyperpolarization-activated channel HCN4 is required for the generation of pacemaker action potentials in the embryonic heart. *Proc Natl Acad Sci U S A*. 2003;100(25):15235–15240.
53. Herrmann S, Stieber J, Stockl G, Hofmann F, Ludwig A. HCN4 provides a 'depolarization reserve' and is not required for heart rate acceleration in mice. *EMBO J*. 2007;26(21):4423–4432.
54. Hoesl E, et al. Tamoxifen-inducible gene deletion in the cardiac conduction system. *J Mol Cell Cardiol*. 2008;45(1):62–69.
55. Herrmann S, Fabritz L, Layh B, Kirchhof P, Ludwig A. Insights into sick sinus syndrome from an inducible mouse model. *Cardiovasc Res*. 2011;90(1):38–48.
56. Berman HM, Ten Eyck LF, Goodsell DS, Haste NM, Kornev A, Taylor SS. The cAMP binding domain: an ancient signaling module. *Proc Natl Acad Sci U S A*. 2005;102(1):45–50.
57. Kannan N, et al. Evolution of allostery in the cyclic nucleotide binding module. *Genome Biol*. 2007;8(12):R264.
58. Kuhlmann MT, et al. G-CSF/SCF reduces inducible arrhythmias in the infarcted heart potentially via increased connexin43 expression and arteriogenesis. *J Exp Med*. 2006;203(1):87–97.
59. Hagendorff A, Schumacher B, Kirchhoff S, Luderitz B, Willecke K. Conduction disturbances and increased atrial vulnerability in Connexin40-deficient mice analyzed by transesophageal stimulation. *Circulation*. 1999;99(11):1508–1515.
60. Knollmann BC, et al. Familial hypertrophic cardiomyopathy-linked mutant troponin T causes stress-induced ventricular tachycardia and Ca2+-dependent action potential remodeling. *Circ Res*. 2003;92(4):428–436.
61. Harzheim D, et al. Cardiac pacemaker function of HCN4 channels in mice is confined to embryonic development and requires cyclic AMP. *EMBO J*. 2008;27(4):692–703.
62. El-Badawi A, Schenk EA. Histochemical methods for separate, consecutive and simultaneous demonstration of acetylcholinesterase and norepinephrine in cryostat sections. *J Histochem Cytochem*. 1967;15(10):580–588.
63. Andree B, et al. Isolation and characterization of the novel popeye gene family expressed in skeletal muscle and heart. *Dev Biol*. 2000;223(2):371–382.
64. Zuzarte M, Rinne S, Schlichthorl G, Schubert A, Daut J, Preisig-Muller R. A di-acidic sequence motif enhances the surface expression of the potassium channel TASK-3. *Traffic*. 2007;8(8):1093–1100.
65. DiAngelo JR, Vasavada TK, Cain W, Duncan MK. Production of monoclonal antibodies against chicken Pop1 (BVES). *Hybrid Hybridomics*. 2001;20(5–6):377–381.
66. Mangoni ME, Nargeot J. Properties of the hyperpolarization-activated current (I(f)) in isolated mouse sino-atrial cells. *Cardiovasc Res*. 2001;52(1):51–64.
67. Stieber J, Wieland K, Stockl G, Ludwig A, Hofmann F. Bradycardic and proarrhythmic properties of sinus node inhibitors. *Mol Pharmacol*. 2006;69(4):1328–1337.